

# Identification of 1,2,5-Oxadiazoles as a New Class of SENP2 Inhibitors Using Structure Based Virtual Screening

Ashutosh Kumar,<sup>†,||</sup> Akihiro Ito,<sup>‡,||</sup> Misao Takemoto,<sup>§</sup> Minoru Yoshida,<sup>‡,§</sup> and Kam Y. J. Zhang<sup>\*,†</sup>

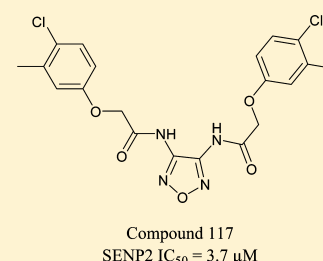
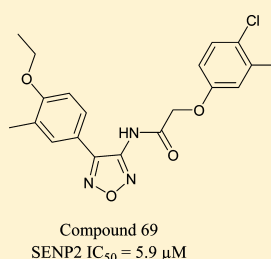
<sup>†</sup>Zhang Initiative Research Unit, RIKEN, 2-1 Hirosawa, Wako, Saitama 351-0198, Japan

<sup>‡</sup>Chemical Genetics Laboratory, RIKEN, 2-1 Hirosawa, Wako, Saitama 351-0198, Japan

<sup>§</sup>Drug Discovery Platform Cooperation Division, RIKEN Center for Sustainable Resource Science, 2-1 Hirosawa, Wako, Saitama 351-0198, Japan

## S Supporting Information

**ABSTRACT:** Small ubiquitin like modifier (SUMO) specific proteases (SENPs) are cysteine proteases that carry out the proteolytic processing of SUMO from its pro form as well as the deconjugation of SUMO from substrate proteins. SENPs are attractive targets for drug discovery due to their crucial role in the development of various diseases. However, the SENPs inhibitor discovery efforts were limited, and only a few inhibitors or activity based probes have been identified until now. Here, we report a new class of SENP2 inhibitors identified by a combination of structure based virtual screening and quantitative FRET based assay. Our virtual screening protocol initially involves the identification of small molecules that have similar shape and electrostatic properties with the conjugate of SUMO1 C-terminal residues and substrate lysine. Molecular docking was then used to prioritize these small molecules for a FRET based assay that quantifies their SENP2 endopeptidase activity. The initial round of virtual screening followed by FRET based assay has enabled the identification of eight compounds with >40% SENP2 inhibition at 30  $\mu$ M compound concentration. Five of these compounds belong to two scaffolds containing a 1,2,5-oxadiazole core that represent a novel class of SENP2 inhibitors. To improve the inhibitory potency and explore the structure–activity relationship of these two 1,2,5-oxadiazole scaffolds, structurally related compounds were identified in another round of virtual screening. The biological assay results confirmed SENP2 inhibitory activity of these two scaffolds. The most potent compound of each scaffold showed an  $IC_{50}$  of 5.9 and 3.7  $\mu$ M. Most of the compounds also inhibited closely related isoform SENP1, while no detectable inhibition on other proteases, such as papain and trypsin, was observed. Our study suggests that 1,2,5-oxadiazoles could be used as a starting point for the development of novel therapeutic agents against various diseases targeting SENPs.



## INTRODUCTION

Sumoylation plays important roles in cellular processes, such as DNA replication and repair, chromosome packing and dynamics, genome integrity, nuclear transport, signal transduction, and cell proliferation.<sup>1–5</sup> Sumoylation involves the covalent attachment of a small ubiquitin like modifier (SUMO) protein to the  $\epsilon$ -amino group of lysine residues in specific target proteins via an enzymatic cascade that requires a sequential action of an activating enzyme E1, a conjugating enzyme E2, and a ligase E3.<sup>1–5</sup> The first step in the sumoylation pathway involves the covalent attachment of adenylated SUMO to the catalytic residue Cys173 on SUMO E1.<sup>6–8</sup> This step requires proteolytic processing of SUMO from its pro form to its mature form.<sup>4,9–12</sup> SUMO specific proteases (SENPs) catalyze the proteolytic processing of SUMOs by cleaving the inactive or pro form of SUMO at the C-terminus via its hydrolase activity to expose two glycine residues and thereby generating active or mature SUMO.<sup>4,9–12</sup> In mammals, six SENPs (SEN1, SEN2, SEN3, SEN5, SEN6, and SEN7) have been identified. These six SENPs differ in their sequence

homology, substrate specificity, and subcellular localization.<sup>4,9–12</sup> All six SENPs also possess isopeptidase activity, and they cleave the isopeptide bond between the C-terminal glycine of SUMO and the substrate protein lysine releasing conjugated SUMO proteins from substrates. This isopeptidase activity of SENPs is essential for the recycling of SUMO proteins.<sup>4,9–12</sup> SENP1 and SENP2 are the most studied isoforms, and their role has been investigated in the development of various diseases including prostate cancer,<sup>13–16</sup> thyroid cancer,<sup>17</sup> colon cancer,<sup>18</sup> atherosclerosis,<sup>19</sup> and heart disease.<sup>20</sup> Overexpression of SENP1 was observed in more than 50% of the studied samples of prostatic intraepithelial neoplasia and prostate cancer.<sup>13,16</sup> SENP1 plays pivotal role in the development of prostate cancer in transgenic mice.<sup>16</sup> Furthermore, high correlation was observed between SENP1 expression and hypoxia-inducing factor 1 $\alpha$  (HIF1 $\alpha$ ) expression,<sup>13</sup> which indicates a role of SENP1 in tumorigenesis. On

Received: December 3, 2013

Published: February 10, 2014

the other hand, SENP2 regulates tumor suppressor p53 by virtue of MDM2 desumoylation.<sup>21,22</sup> Also, SENP2 modulates the stability of  $\beta$ -catenin to regulate hepatocellular carcinoma cell growth.<sup>23</sup> Moreover, SENP2 regulates the sumoylation levels of p53 and extracellular signal-regulated kinase-5 (ERK5) under disturbed flow conditions and contributes to atherosclerotic plaque formation.<sup>19</sup> Furthermore, it has been reported that the overexpression of SENP2 gave rise to congenital heart defects and cardiac dysfunction in murine hearts.<sup>20</sup>

The above studies suggest that SENPs can be attractive targets for drug discovery due to their crucial role in the development of various diseases. However, until now the SENP inhibitor discovery efforts were limited, and only a few inhibitors or activity based probes have been identified for SENPs.<sup>24–31</sup> Some of these inhibitors were developed using a full or truncated form of SUMO carrying electrophilic trap, i.e., a reactive functional group such as vinyl sulfones at the C-terminal glycine.<sup>24,25</sup> Another class consists of small molecular or peptidyl SENP inhibitors and activity based probes developed recently.<sup>26–28</sup> All of these inhibitors possess reactive chemical functionalities that bind covalently to the active site cysteine. These include SENP inhibitors containing azaepoxide and acyloxymethyl ketone reactive groups,<sup>26</sup> a formyl group containing benzodiazepines,<sup>27</sup> and a few peptidyl active site probes harboring a glycine derived fluoromethylketone moiety at its C-terminus.<sup>28</sup> Recently, 2-(4-chlorophenyl)-2-oxoethyl 4-benzamidobenzoate derivatives and 1-[4-(N-benzylamino)phenyl]-3-phenylurea derivatives have been reported as new classes of nonpeptidic SENP1 inhibitors.<sup>29,30</sup> Furthermore, a new class of SENPs inhibitors has been recently reported that do not covalently modify the catalytic cysteine.<sup>31</sup> Although some of the reported SENP inhibitors are fairly potent,<sup>24–31</sup> to fully exploit the therapeutic potential of SENP inhibitors, more chemical scaffolds are required. Under these circumstances, it is desirable to identify inhibitors with new chemical scaffolds for the study of therapeutic and biological roles of SENPs in various diseases.

Here, we report the identification of 1,2,5-oxadiazoles as a new class of SENP2 inhibitors using structure based virtual screening followed by biological assay. The 1,2,5-oxadiazoles also inhibited closely related isoform SENP1 but do not exhibit noticeable activity against other proteases such as cysteine protease papain and serine protease trypsin. Our study suggests that 1,2,5-oxadiazoles can be used as starting points for the development of highly potent SENP inhibitors for therapeutic and biological purposes.

## MATERIALS AND METHODS

**Shape and Electrostatic Similarity Search.** The crystal structure of SENP2 in complex with SUMO1 and RanGAP1 (PDB code 2IO2)<sup>32</sup> was used to prepare a query for a shape and electrostatic similarity search against ~4 million compounds in the Namiki-shoji small molecule library (<http://www.namiki-s.co.jp>). The query consisting of three C-terminal amino acids Thr95, Gly96, and Gly97 from SUMO1 and Lys524 from substrate RanGAP1 was used to retrieve compounds matching the three-dimensional shape and electrostatic properties. ROCS<sup>33</sup> was used to perform three-dimensional alignment and shape comparisons. TanimotoCombo values were used to rank compounds, and 1000 hits were selected for electrostatic comparisons. The EON program<sup>34</sup> was used to further filter compounds with matching electrostatic profiles. The electrostatic similarity score (ET\_combo)

from EON was used to rank compounds, and 500 hits were selected for further prioritization. Electrostatic matching calculations were performed using MMFF94 partial charges.<sup>35,36</sup>

**Preparation of Receptor and Small Molecule Library for Molecular Docking.** Preparation of the receptor structure for docking calculations was accomplished using the protein preparation utility of Schrodinger's Maestro.<sup>37</sup> The SENP2 crystal structure in complex with SUMO1 and RanGAP1 (PDB code 2IO2)<sup>32</sup> was used for molecular docking. To prepare receptor structures, hydrogens were added, bond orders were assigned, and all the water molecules except those within a 4.5 Å vicinity of the SUMO C-terminal peptide fragment were removed. Protonation states of charged residues were determined using Schrodinger's Maestro.<sup>37</sup> Hits selected after the shape and electrostatic similarity search were prepared for docking using LigPrep.<sup>38</sup> Hydrogen atoms were added, ionizations states were generated, and tautomers were generated to prepare structures. All structures were subjected to minimization using the OPLS-2005 force field.<sup>39,40</sup>

**Molecular Docking.** All of the molecular docking calculations were performed by Glide version 5.7 interfaced with the Schrodinger suite using extra precision mode (Glide-XP).<sup>41–44</sup> Grids for molecular docking calculations were generated by using sites defined by the centroid of query used for shape and electrostatic similarity calculations. Docking was carried out using default settings. Glide-XP score<sup>41–44</sup> was used to rank compounds. The docking results were analyzed using Glide-XP visualizer. The PyMOL molecular graphics program<sup>45</sup> was used to prepare the graphics.

**Biological Assay.** The FRET based assay for quantitatively measuring the SENPs activity was performed as described.<sup>46</sup> Briefly, the recombinant CyPet–pre-SUMO-1–YPet protein was incubated with the recombinant catalytic domain of SENP1 or SENP2 for 1 h at 37 °C in a buffer containing 25 mM Tris–HCl (pH 8.0), 150 mM NaCl, 0.1% Tween 20, and 2 mM DTT, and the fluorescence intensity of the solution was measured at emission wavelengths of 475 nm for CyPet and 530 nm for YPet with an excitation wavelength of 414 nm using a SpectraMax M2 microplate reader (Molecular Devices).

The enzymatic activity of papain was conducted by measuring the emission intensity of FICT-casein at 520 nm with an excitation wavelength of 490 nm. Briefly, the papain protein (SIGMA) was incubated with 10  $\mu$ M FICT-casein (AnaSpec) for 1 h at 37 °C in a buffer containing 50 mM Tris–HCl (pH 7.4), and the fluorescence intensity of the solution was measured using a SpectraMax M2 microplate reader.

For measuring the enzymatic activity of trypsin, the trypsin protein (Affymetrix) was incubated with 40  $\mu$ M Boc-Lys-MCA for 1 h at 37 °C in a buffer containing 20 mM Tris–HCl (pH 7.4), 150 mM NaCl, and 10% glycerol, and the fluorescence intensity of the solution was measured at an excitation wavelength of 370 nm and a fluorescence wavelength of 460 nm with a SpectraMax M2 microplate reader.

**Compounds.** Tested compounds were purchased from several chemical vendors (Enamine, Vitas-M, Princeton, Life Chemicals, Asinex, Scientific Exchange, SALOR, Pharmeks and Zelinsky Institute) via a local distributor. The vendors have verified that each compound had more than 95% purity by liquid chromatography–mass spectrometry and NMR experiments. Compounds were maintained as a DMSO stock solution.

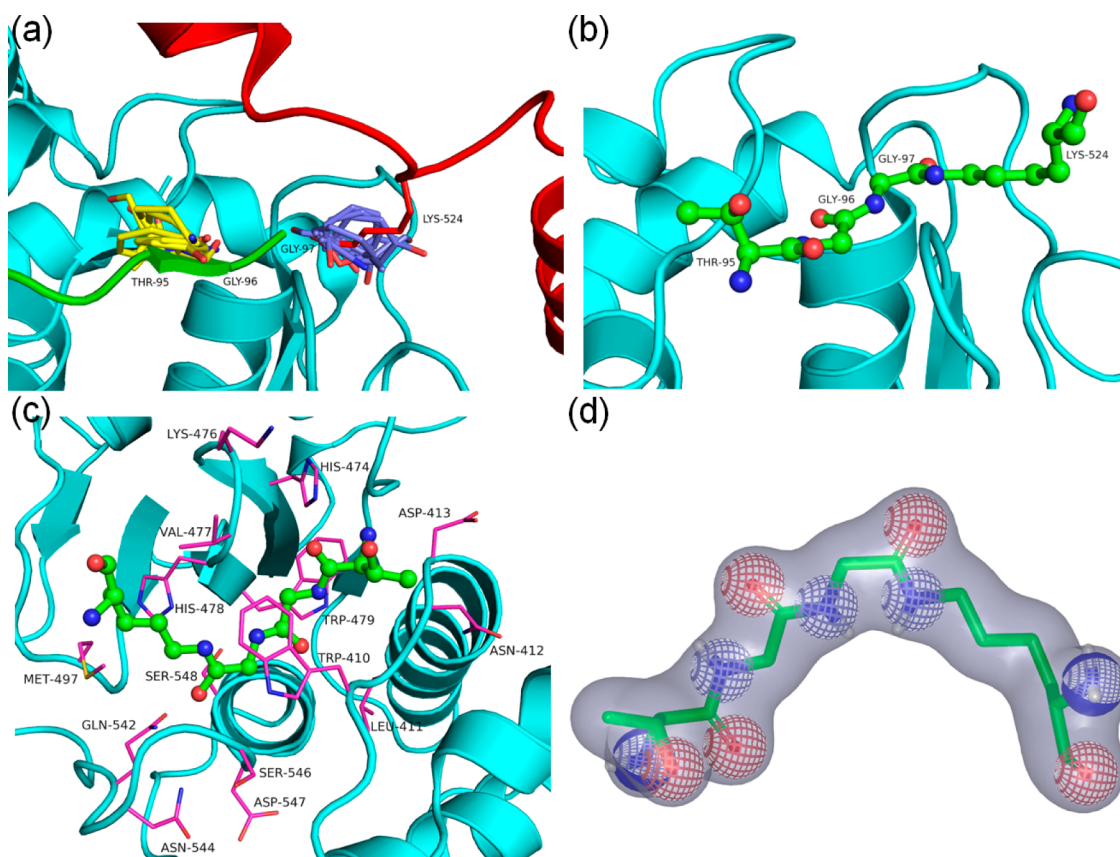


**Figure 1.** Generation of a query for shape and electrostatic matching calculations. (a) Overlay of FTMap consensus sites (CSs) on the SENP2–SUMO1–RanGAP1 protein complex (PDB code 2IO2). (b) Peptide fragment consisting of Thr95, Gly96, and Gly97 from SUMO1 and Lys524 from substrate RanGAP1. (c) Peptide fragment in SENP2 catalytic site. (d) Query for the shape and electrostatic potential matching calculation. Red and blue spheres represent “color” chemical features.

## RESULTS AND DISCUSSION

**Generation of Query for Shape and Electrostatic Similarity Search.** The shape-based and electrostatic similarity based screenings are established ligand-based virtual screening tools.<sup>47–49</sup> These approaches involve the overlay of compounds in a screening database onto one or few query molecules, which is followed by the calculation of similarity in three-dimensional shape and electrostatic properties. It has been previously reported that the selection of an appropriate query for shape-based and electrostatic similarity based screening is very important as it affects the virtual screening performance.<sup>50,51</sup> In most cases, the query for the shape and electrostatic similarity search is generated from highly potent small molecule inhibitors of the protein under study.<sup>48,49,52</sup> However, we have chosen not to use the reported SENP inhibitors<sup>24–31</sup> for preparing a query for shape and electrostatic similarity based virtual screening for three reasons: (1) There was no crystal structure of any SENP isoform with bound inhibitor, so the bioactive conformation of these inhibitors is not known. (2) Most of the reported SENP inhibitors contain an electrophilic trap or “warhead” which drives the activity of these compounds. Using these compounds as a query will mostly retrieve similar compounds. (3) As most of the known SENP inhibitors have high molecular weight, shape similarity screening will also retrieve high molecular weight compounds. Such high molecular weight compounds are difficult to optimize for drug-like properties and hence not desired in our screening campaign. Recently reported noncovalent SENP inhibitors<sup>31</sup>

were not considered as they were unavailable when this study was carried out. Instead, the query for shape and electrostatic matching was prepared from sumoylated substrate RanGAP1 bound to SENP2.

The crystal structure of SENP2 in complex with SUMO1 and RanGAP1 (PDB code 2IO2)<sup>32</sup> was used to prepare a query for a shape and electrostatic similarity search. Query generation was facilitated by performing computational fragment mapping calculations on the SENP2 catalytic site using the FTMap server.<sup>53</sup> This has resulted in two highly populated consensus sites (CSs) at the SENP2 catalytic site, which is shown in Figure 1a. These two CSs lie over the SUMO1 C-terminus conjugated with Lys524 of RanGAP1. As seen in Figure 1a, one of the CSs overlaps with the Lys524 side chain of substrate protein RanGAP1, while the other overlaps with the Thr95 of SUMO1. Figure 1b illustrates these three C-terminal amino acids Thr95, Gly96, and Gly97 from SUMO1 and Lys524 from substrate RanGAP1 (TGGK fragment), which were then used to prepare a query using vROCS.<sup>33</sup> The TGGK fragment is stacked between Trp410 and Trp479 and forms hydrogen bonds with the backbone of Val477 in SENP2 (Figure 1c). These stacking interactions and hydrogen bonds are expected to be conserved for compounds with similar shape and electrostatic properties. The query generated using vROCS for shape matching calculations is shown in Figure 1d, which illustrates the 3D shape with chemical features (known as “color” in ROCS) used to refine shape overlays.



**Hierarchical Structure Based Virtual Screening Procedure.** To identify SENP2 inhibitors targeting the catalytic site, a hierarchical structure based virtual screening procedure was employed first and then followed by biological testing of the identified compounds. The virtual screening procedure is summarized in Figure 2. It starts with the generation of a query

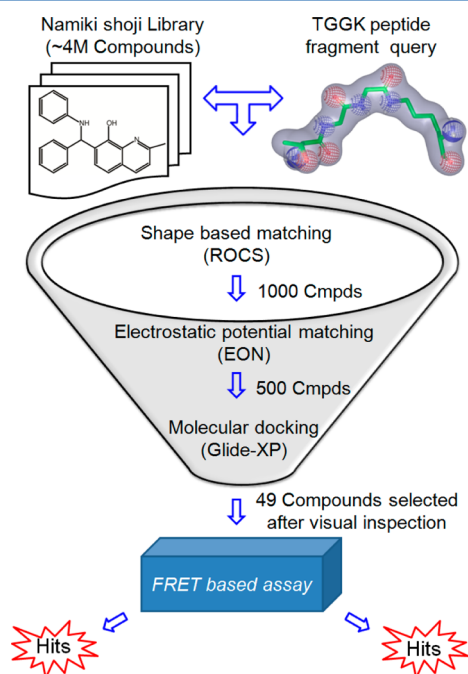


**Figure 2.** An overview of the in silico screening protocol used to identify SENP2 inhibitors. Initially, a peptide fragment query generated from the SENP2–SUMO1–RanGAP1 complex structure was used to identify compounds with matching shape and electrostatic properties. The compounds with matching profiles were further prioritized by molecular docking. Compounds selected after visual inspection were acquired and tested using a FRET based assay to measure their inhibition of SENP2 endopeptidase activity.

for shape and electrostatic similarity search as mentioned previously. The query consisting of amino acid residues Thr95, Gly96, and Gly97 of SUMO1 and Lys524 from substrate RanGAP1 generated using vROCS was used for three-dimensional shape and electrostatic matching using ROCS<sup>33</sup> and the EON program.<sup>34</sup> Virtual screening was then carried out against the Namiki-shoji small molecule library, which is a collection of ~4 million commercially available compounds from various chemical vendors. Prior to screening, a conformational database of the Namiki shoji library with a maximum of 200 conformations for each compound was generated using OMEGA.<sup>54–56</sup> Initially, each molecule in the Namiki-shoji conformational database was aligned with the query and scored for three-dimensional shape overlap using ROCS.<sup>33</sup> The shape based overlays were refined using “color” features of ROCS, which is a measure of chemical similarity between the query and screening database molecule. TanimotoCombo ( $T_C$ ), a combined Tanimoto coefficient<sup>57</sup> for shape overlap (Shape-Tanimoto) and color overlap (ColorTanimoto), was used to score molecules. The top 1000 hits ranked according to decreasing  $T_C$  were saved for further analysis. The  $T_C$  values for 1000 hit compounds ranged from 0.995 to 0.852, while the mean  $T_C$  value was 0.874.

To complement the shape based screening and to further prioritize 1000 hits obtained after ROCS screening, electrostatic potential matching calculations were carried out using the EON<sup>34</sup> program. As EON requires molecules to be prealigned with the query for electrostatic comparison, previous ROCS calculations were run with the “eon\_input” flag to prepare input for EON calculations. ET\_combo score, a combination score for electrostatics match and shape match, was used to rank compounds. On the basis of decreasing values, the top 500 hit compounds were saved. The ET\_combo values for 500 hit compounds ranged from 1.455 to 0.749, while the mean ET\_combo value was 0.899.

To further prioritize hits for a biological assay, the top 500 hits with matching shape and electrostatic potential with the query (TGGK fragment) were analyzed for geometric and energetic complementarity with catalytic site residues by molecular docking. Molecular dockings were accomplished using Glide-XP.<sup>41–44</sup> The SENP2 catalytic site consisting of Trp410, Leu411, Asn412, His474, Lys476, Val477, His478, Trp479, Met497, Gln542, Gly545, Ser546, Asp547, Ser548, and Gly549 amino acid residues was selected as a target area for molecular docking. The compounds were ranked using the Glide-XP scoring function, and the top 200 hits were visualized using Glide-XP visualizer and analyzed for the interactions they make with active site residues. The Glide-XP score ranged from −9.44 to −1.87 for the top 200 compounds. There was no correlation between the Glide-XP score and molecular weight, so the compounds that were ranked higher indeed formed good interactions. The correlation plot between Glide-XP score and molecular weight is given as Supporting Information Figure S1.

The visual analysis of the top 200 hits revealed 1,2,5-oxadiazoles as a major chemical class accounting for 34.5% of the top ranking hits (Supporting Information Figure S2). These 1,2,5-oxadiazole compounds comprise two substructures, namely, 2-phenoxy-N-[4-(2-phenoxyacetyl amino)(1,2,5-oxadiazol-3-yl)]acetamide and 2-phenoxy-N-(4-phenyl-1,2,5-oxadiazol-3-yl)acetamide. The enrichment of 1,2,5-oxadiazoles as top ranking compounds in our virtual screening campaign was not due to the quality of our screening library, as a substructure search using a 1,2,5-oxadiazole core could retrieve only 0.2% of the compounds out of the ~4 million compounds library. One possible reason for the enrichment of 1,2,5-oxadiazoles ahead of other chemical classes would be their ability to form similar interactions as the query TGGK fragment (Supporting Information Figure S2). The TGGK fragment forms both hydrogen bonding and hydrophobic interactions. Lys524 is involved in the formation of hydrophobic contacts via its hydrocarbon side chain with Met497 and Val477. In addition, the main chain amides in Gly96 and Gly97 of the TGGK fragment form hydrogen bonds with the backbone carbonyl of Val477 (Figure 1c). The docking predicted binding mode of 1,2,5-oxadiazoles suggests that these interactions were well conserved. The hydrogen bond with Val477 was the most prominent as 161 out of top 200 hits showed this interaction. These interactions along with others such as hydrogen bonding with Gln542 were then used to prioritize compounds for biological assay. Some representative compounds belonging to 1,2,5-oxadiazoles were chosen based on docking scores, and hits other than 1,2,5-oxadiazoles were clustered together, and representative molecules for each class were selected. Finally, a set of 49 compounds was selected and purchased from commercial vendors for biological assay.

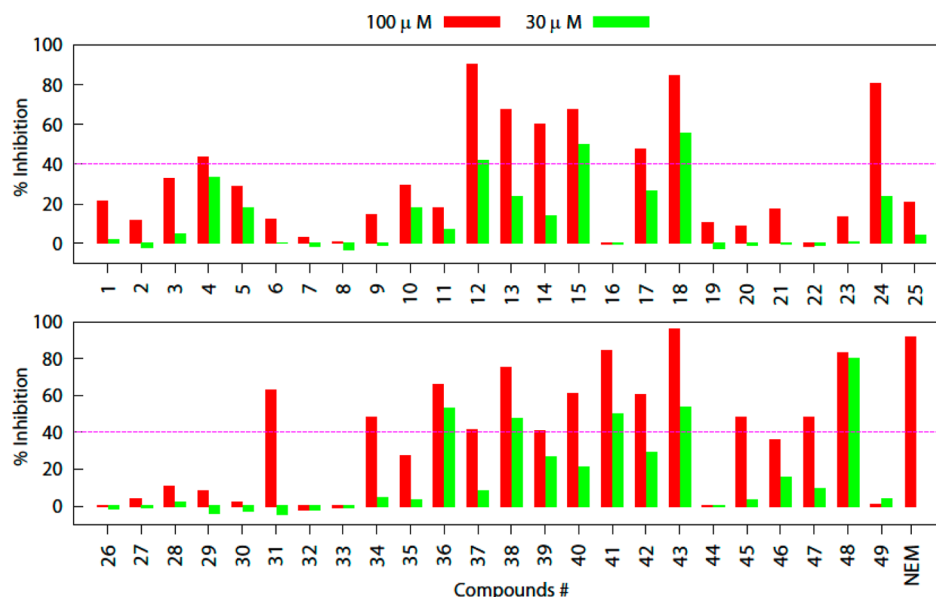


**Figure 3.** A quantitative FRET based assay to evaluate the inhibition of *in vitro* SENP2 endopeptidase activity by virtual screening hits. The compounds were tested for inhibition of SENP2 endopeptidase activity at 100 and 30  $\mu\text{M}$ , while 100  $\mu\text{M}$  N-ethylmaleimide (NEM) was used as a positive control for the experiment.

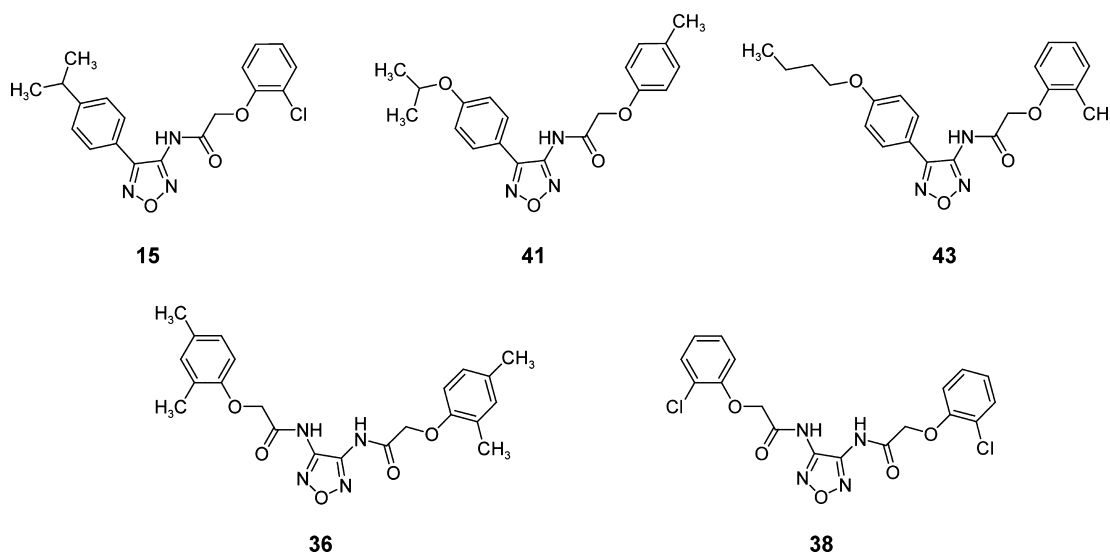


**Figure 4.** Chemical structures of the first round virtual screening hits with a 1,2,5-oxadiazole core.

**FRET Based Biological Assay.** To evaluate the *in vitro* SENP2 endopeptidase activity of 49 hits selected and acquired after virtual screening, we developed a quantitative FRET based assay as previously described.<sup>46</sup> The compounds were tested for inhibition of SENP2 endopeptidase activity at 100 and 30  $\mu\text{M}$ , while 100  $\mu\text{M}$  N-ethylmaleimide (NEM), a cysteine protease inhibitor, was used as a positive control for the experiment. Fourteen compounds (12–15, 18, 24, 31, 36, 38, 40–43, and 48) inhibited at least 60% of SENP2 endopeptidase activity at the concentration of 100  $\mu\text{M}$ , with six of them (12, 18, 24, 41, 43, and 48) inhibiting at least 80% of the endopeptidase activity (Figure 3). These compounds were further tested to check their ability to inhibit SENP2 activity at a lower concentration of 30  $\mu\text{M}$ . Eight compounds (12, 15, 18, 36, 38, 41, 43, and 48) showed more than 40% inhibition of SENP2 endopeptidase activity. Five out of eight compounds (15, 36, 38, 41, and 43) contain a 1,2,5-oxadiazoles scaffold which represents a

novel chemical class displaying potency against SENP2. The chemical structures of 15, 36, 38, 41, and 43 are presented in Figure 4. Among these five compounds, three compounds (15, 41, and 43) share a 2-phenoxy-N-(4-phenyl-1,2,5-oxadiazol-3-yl)acetamide scaffold while two compounds (36 and 38) share a 2-phenoxy-N-[4-(2-phenoxyacetamido)(1,2,5-oxadiazol-3-yl)]acetamide scaffold. These two scaffolds represent an interesting chemical class for further exploration. Therefore, we decided to further optimize the SENP2 inhibitory activities of the 2-phenoxy-N-(4-phenyl-1,2,5-oxadiazol-3-yl)acetamide and 2-phenoxy-N-[4-(2-phenoxyacetamido)(1,2,5-oxadiazol-3-yl)]acetamide scaffolds.

In order to improve potency and explore the structure–activity relationship of 2-phenoxy-N-(4-phenyl-1,2,5-oxadiazol-3-yl)acetamide and 2-phenoxy-N-[4-(2-phenoxyacetamido)(1,2,5-oxadiazol-3-yl)]acetamide scaffolds, another round of shape and electrostatic similarity search was carried out against

Table 1. Structure and Inhibitory Activities of 2-Phenoxy-N-(4-phenyl-1,2,5-oxadiazol-3-yl)acetamides

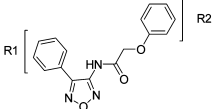
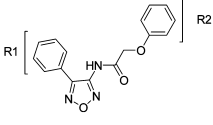
Cmpds	Structure		SENP2				SENP1		Papain		Trypsin	
			% inhibition at 10 $\mu$ M	% inhibition at 20 $\mu$ M	IC <sub>50</sub> ( $\mu$ M)	SD	IC <sub>50</sub> ( $\mu$ M)	SD	% of control at 100 $\mu$ M	SD	% of control at 100 $\mu$ M	SD
												
	R1	R2										
43	4-O-butyl	2-CH <sub>3</sub>	21.2	43.3	12.4	3.2	>30	-	119.2	11.3	107.4	3.5
50	3,4-CH <sub>3</sub>	3,4-CH <sub>3</sub>	6.4	13.5	-	-	-	-	-	-	-	-
51	3,4-CH <sub>3</sub>	3-CH <sub>3</sub>	7.6	18.9	-	-	-	-	-	-	-	-
52	3,4-CH <sub>3</sub>	3-CH <sub>3</sub> , 4-Cl	29.7	39.7	6.8	1.1	6.4	1.2	113.5	19.6	107.6	5.3
53	3,4-CH <sub>3</sub>	3-Cl	20.1	38.0	-	-	-	-	-	-	-	-
54	3,4-OCH <sub>2</sub> CH <sub>3</sub>	3,5-CH <sub>3</sub> , 4-Cl	47.1	40.9	>30	-	>30	-	99.4	13.2	104.3	4.9
55	3,4-OCH <sub>2</sub> CH <sub>3</sub>	4-CH <sub>3</sub>	6.5	26.7	-	-	-	-	-	-	-	-
56	3,4-OCH <sub>2</sub> CH <sub>3</sub>	4-Cl	19.9	29.6	-	-	-	-	-	-	-	-
57	3,4-OCH <sub>2</sub> CH <sub>3</sub>	3-CH <sub>3</sub>	7.5	12.6	-	-	-	-	-	-	-	-
58	3,4-OCH <sub>2</sub> CH <sub>3</sub>	4-F	5.8	16.9	-	-	-	-	-	-	-	-
59	3,4-OCH <sub>2</sub> CH <sub>3</sub>	2-CH <sub>3</sub> , 4-Cl	30.8	44.5	7.6	0.4	7.0	1.8	110.6	14.6	104.4	1.0
60	3,4-OCH <sub>3</sub>	3-CH <sub>3</sub>	-5.9	0.5	-	-	-	-	-	-	-	-
61	3,4-OCH <sub>3</sub>	3,5-CH <sub>3</sub> , 4-Cl	14.2	25.9	-	-	-	-	-	-	-	-
62	3,4-OCH <sub>3</sub>	4-CH <sub>3</sub>	-4.0	3.4	-	-	-	-	-	-	-	-
63	3,4-OCH <sub>3</sub>	3,5-CH <sub>3</sub>	10.4	16.2	-	-	-	-	-	-	-	-
64	3,4-OCH <sub>3</sub>	3,4-CH <sub>3</sub>	-1.6	6.3	-	-	-	-	-	-	-	-
65	3,4-OCH <sub>3</sub>	3-CH <sub>3</sub> , 4-Cl	18.3	26.6	-	-	-	-	-	-	-	-
66	3,4-OCH <sub>3</sub>	4-Cl	-7.5	3.9	-	-	-	-	-	-	-	-
67	3-CH <sub>3</sub> , 4-OCH <sub>2</sub> CH <sub>3</sub>	3-CH <sub>3</sub>	9.3	13.7	-	-	-	-	-	-	-	-
68	3-CH <sub>3</sub> , 4-OCH <sub>2</sub> CH <sub>3</sub>	3-Cl	26.3	52.9	8.7	1.3	10.7	2.5	106.6	5.1	108.7	4.6
69	3-CH <sub>3</sub> , 4-OCH <sub>2</sub> CH <sub>3</sub>	3-CH <sub>3</sub> , 4-Cl	33.4	41.2	5.9	1.3	9.7	3.0	104.2	6.8	106.7	5.0
70	3-CH <sub>3</sub> , 4-OCH <sub>3</sub>	2-Cl	8.0	20.0	-	-	-	-	-	-	-	-
71	3-CH <sub>3</sub> , 4-OCH <sub>3</sub>	2,3-CH <sub>3</sub>	11.2	20.9	-	-	-	-	-	-	-	-
72	3-CH <sub>3</sub> , 4-OCH <sub>3</sub>	3,5-CH <sub>3</sub>	8.9	25.8	-	-	-	-	-	-	-	-
73	3-CH <sub>3</sub> , 4-OCH <sub>3</sub>	4-isopropyl	14.9	13.8	-	-	-	-	-	-	-	-
74	3-CH <sub>3</sub> , 4-OCH <sub>3</sub>	2-OCH <sub>3</sub>	-4.6	7.0	-	-	-	-	-	-	-	-
75	4-CH <sub>3</sub>	3-Cl	-0.2	13.2	-	-	-	-	-	-	-	-
76	4-Cl	4-F	-4.9	-1.0	-	-	-	-	-	-	-	-
77	4-F	2-CH <sub>3</sub>	-4.2	1.5	-	-	-	-	-	-	-	-
78	4-O-butyl	4-CH <sub>3</sub>	20.0	39.6	9.4	2.9	>30	-	118.2	10.6	109.0	3.0
79	4-O-butyl	2-F	10.7	15.7	-	-	-	-	-	-	-	-
80	4-OCH <sub>2</sub> CH <sub>3</sub>	4- <i>t</i> -butyl	13.0	18.5	-	-	-	-	-	-	-	-
81	4-OCH <sub>2</sub> CH <sub>3</sub>	2-CH <sub>3</sub>	5.4	22.8	-	-	-	-	-	-	-	-
82	4-OCH <sub>2</sub> CH <sub>3</sub>	2-CH <sub>3</sub> , 4-Cl	38.2	55.2	14.0	3.6	21.6	8.9	106.0	17.5	106.5	4.3
83	4-OCH <sub>2</sub> CH <sub>3</sub>	4-Cl	28.4	49.5	10.7	1.5	12.7	4.9	113.8	12.5	104.0	3.0
84	4-OCH <sub>2</sub> CH <sub>3</sub>	2,3-CH <sub>3</sub>	33.0	56.7	17.4	5.5	>30	-	104.6	18.2	110.7	4.9

Table 1. continued

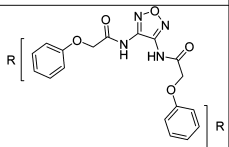
Cmpds	Structure		SEN2				SEN1		Papain		Trypsin	
			% inhibition at 10 $\mu$ M	% inhibition at 20 $\mu$ M	IC <sub>50</sub> ( $\mu$ M)	SD	IC <sub>50</sub> ( $\mu$ M)	SD	% of control at 100 $\mu$ M	SD	% of control at 100 $\mu$ M	SD
												
	R1	R2										
85	4-OCH <sub>2</sub> CH <sub>3</sub>	4-Br	23.5	41.0	17.3	4.1	24.2	6.3	98.1	15.9	106.5	3.9
86	4-OCH <sub>2</sub> CH <sub>3</sub>	3,5-CH <sub>3</sub> , 4-Cl	28.1	31.3	-	-	-	-	-	-	-	-
87	4-OCH <sub>3</sub>	3,5-CH <sub>3</sub>	6.3	17.0	-	-	-	-	-	-	-	-
88	4-OCH <sub>3</sub>	2-isopropyl, 5-CH <sub>3</sub>	12.7	12.9	-	-	-	-	-	-	-	-
89	4-OCH <sub>3</sub>	3-CH <sub>3</sub>	-6.9	3.3	-	-	-	-	-	-	-	-
90	4-OCH <sub>3</sub>	4-Br	-0.3	6.5	-	-	-	-	-	-	-	-
91	4-OCH <sub>3</sub>	3,5-CH <sub>3</sub> , 4-Cl	30.4	38.6	7.7	1.1	16.6	8.7	116.0	10.6	106.2	2.3
92	4-OCH <sub>3</sub>	2-OCH <sub>3</sub>	-8.0	-2.6	-	-	-	-	-	-	-	-
93	4-OCH <sub>3</sub>	3-Cl	-3.8	3.8	-	-	-	-	-	-	-	-
94	4-OCH <sub>3</sub>	3,4-CH <sub>3</sub>	-3.8	7.9	-	-	-	-	-	-	-	-
95	4-OCH <sub>3</sub>	2-CH <sub>3</sub>	-4.7	8.5	-	-	-	-	-	-	-	-
96	4-OCH <sub>3</sub>	3-CH <sub>3</sub> , 4-Cl	6.9	24.4	-	-	-	-	-	-	-	-
97	4-OCH <sub>3</sub>	2-F	-7.6	-0.9	-	-	-	-	-	-	-	-
98	4-O-isobutyl	4-Cl	39.7	52.9	7.8	2.3	18.5	2.7	109.7	4.6	106.4	0.9
99	4-O-isobutyl	2-Cl	21.4	32.7	-	-	-	-	-	-	-	-
100	4-O-isobutyl	2-OCH <sub>3</sub>	26.6	29.6	-	-	-	-	-	-	-	-
101	4-O-isobutyl	4-F	24.8	40.0	7.5	0.9	6.0	1.1	116.0	5.1	105.5	2.7
102	4-O-isobutyl	4-CH <sub>2</sub> CH <sub>3</sub>	28.7	40.2	6.3	0.3	13.7	0.3	116.9	5.3	108.6	3.4
103	4-O-isobutyl	2,3-CH <sub>3</sub>	22.8	32.6	-	-	-	-	-	-	-	-
104	4-O-isopropyl	3-CH <sub>3</sub>	6.5	20.3	-	-	-	-	-	-	-	-
105	4-O-isopropyl	H	-2.9	9.6	-	-	-	-	-	-	-	-
106	4-O-isopropyl	3,5-CH <sub>3</sub>	27.1	45.2	8.2	1.2	19.8	11.9	118.0	11.2	109.2	2.7
107	4-O-isopropyl	3-CH <sub>3</sub> , 4-Cl	42.7	56.5	6.3	1.2	6.2	1.7	120.9	10.5	103.0	1.9
108	4-O-isopropyl	2-CH <sub>3</sub> , 4-Cl	16.2	44.1	6.2	0.4	9.6	4.2	111.0	5.8	103.9	1.9
109	4-O-isopropyl	2,4-Cl	31.1	72.1	9.0	1.2	7.9	2.8	106.1	4.0	106.1	4.9
110	4-O-propyl	3-CH <sub>3</sub>	31.8	45.3	15.7	4.5	>30	-	105.2	18.9	106.6	2.8
111	4-O-propyl	3-CH <sub>3</sub> , 4-Cl	36.0	58.8	7.0	1.8	9.9	4.4	116.5	13.8	106.4	1.8
112	4-O-propyl	4-Cl	30.9	44.5	11.0	3.8	11.5	0.2	111.0	18.9	105.4	4.5
113	4-O-propyl	H	2.4	23.5	-	-	-	-	-	-	-	-
114	4-O-propyl	3,4-CH <sub>3</sub>	22.3	35.7	-	-	-	-	-	-	-	-

the Namiki-shoji collection of commercially available compounds. This time, the representative compounds for 2-phenoxy-N-(4-phenyl-1,2,5-oxadiazol-3-yl)acetamide and 2-phenoxy-N-[4-(2-phenoxyacetyl amino)(1,2,5-oxadiazol-3-yl)]acetamide (compound 43 and 38) were used as a query for similarity search instead of a TGGK fragment with a similar protocol as mentioned previously. The compounds sharing shape and electrostatic similarity with compounds 43 and 38 were further prioritized by molecular docking using Glide-XP.<sup>41–44</sup> Finally, another set of 65 and 15 compounds each

sharing a 2-phenoxy-N-(4-phenyl-1,2,5-oxadiazol-3-yl) acetamide and 2-phenoxy-N-[4-(2-phenoxyacetyl amino)(1,2,5-oxadiazol-3-yl)]acetamide scaffold were selected for a biological assay. The compounds were acquired from the chemical vendors and tested at 10 and 20  $\mu$ M using the FRET based assay as described previously.

The results of the biological assay of 65 2-phenoxy-N-(4-phenyl-1,2,5-oxadiazol-3-yl) acetamide derivatives revealed that 20 compounds (52, 54, 59, 68, 69, 78, 82–85, 98, 101, 102, and 106–112) inhibited at least 40% of SENP2 endopeptidase

Table 2. Structure and Inhibitory Activities of 2-Phenoxy-N-[4-(2-phenoxyacetyl amino)(1,2,5-oxadiazol-3-yl)]acetamides

Cmpds	Structure	SENP2				SENP1		Papain		Trypsin	
		% inhibition at 10 $\mu$ M	% inhibition at 20 $\mu$ M	IC <sub>50</sub> ( $\mu$ M)	SD	IC <sub>50</sub> ( $\mu$ M)	SD	% of control at 100 $\mu$ M	SD	% of control at 100 $\mu$ M	SD
											
	<b>R</b>										
38	2-Cl	13.92	35.70	12.2	0.5	28.1	10.8	105.1	6.1	104.6	3.2
115	2- <i>s</i> -butyl	39.37	57.9	4.5	1.2	4.4	4.3	110.5	19.8	98.2	4.3
116	2,6-CH <sub>3</sub> , 4-Br	34.32	47.64	12.7	1.7	9.7	-	105.3	21.8	102.5	6.9
117	3-CH <sub>3</sub> , 4-Cl	54.88	19.89	3.7	0.5	>30	-	97.9	7.5	103.4	3.4
118	4-Br	58.56	69.48	6.8	1.3	15.9	5.1	97.5	5.4	105.5	4.6
119	2,5-CH <sub>3</sub>	32.20	42.00	6.3	0.9	8.1	1.6	106.0	16.8	106.9	4.6
120	4-Cl	52.10	72.63	5.0	0.5	4.7	0.7	62.9	5.4	101.2	0.5
121	3,5-CH <sub>3</sub> , 4-Cl	38.02	58.58	4.4	0.7	13.2	4.5	56.6	8.5	104.5	3.0
122	4-isopropyl	80.82	86.40	4.0	1.0	4.5	3.1	94.0	9.5	106.0	0.9
123	3-CH <sub>3</sub> , 6-isopropyl	51.16	58.26	5.2	1.2	5.4	3.6	115.3	9.2	104.9	1.0
124	3,5-CH <sub>3</sub>	69.74	82.97	5.9	0.2	15.5	4.8	92.0	14.0	102.9	1.9
125	3-CH <sub>3</sub>	13.41	32.66	-	-	-	-	-	-	-	-
126	4-OCH <sub>3</sub>	-1.08	8.00	-	-	-	-	-	-	-	-
127	2-CH <sub>3</sub>	31.81	38.03	-	-	-	-	-	-	-	-
128	4-CH <sub>2</sub> CH <sub>3</sub>	76.08	93.00	14.1	4.6	>30	-	81.8	9.9	102.7	3.1
129	4-CH <sub>3</sub>	44.45	60.97	11.6	7.8	>30	-	98.4	17.8	104.2	5.7

activity (Table 1) at a 20  $\mu$ M compound concentration, confirming the validity of the 1,2,5-oxadiazole scaffold as SENP2 inhibitors. The activity of these 20 compounds was further confirmed by a dose dependent assay at 0.3, 1, 3, 10, and 30  $\mu$ M compound concentrations. The IC<sub>50</sub> was determined from three independent experiments and reported as mean  $\pm$  SD. Compound **91** was also tested since it showed more than 30% inhibition at 10  $\mu$ M. The IC<sub>50</sub> values are presented in Table 1, which shows that 16 compounds (**52**, **59**, **68**, **69**, **78**, **83**, **91**, **98**, **101**, **102**, **106–109**, **111**, and **112**) displayed slightly higher activities than parent compound **43**. Compound **69** was found to be most active among the 2-phenoxy-N-(4-phenyl-1,2,5-oxadiazol-3-yl) acetamide scaffold with an IC<sub>50</sub> value of 5.9  $\mu$ M.

The results of biological activities of 2-phenoxy-N-(4-phenyl-1,2,5-oxadiazol-3-yl) acetamide derivatives prompted us to investigate the structure–activity relationship (SAR) of virtually screened compounds with different substituents on the 2-phenoxy-N-(4-phenyl-1,2,5-oxadiazol-3-yl)acetamide scaffold. Specifically, substitutions in these compounds were available at different positions of two phenyls on either side of the 1,2,5-oxadiazole core (R1 and R2 in Table 1). The preliminary SAR investigation (Table 1) has shown that an electron-withdrawing group at position 4 of R2 is essential to achieve significant inhibition of SENP2 endopeptidase activity. The substitution of chloro at position 4 of R2 resulted in significant improvement in the potency of compounds **52**, **59**, **69**, **82**, **83**, **91**, **98**, **107–**

**109**, **111**, and **112**. In fact, more than 60% of the compounds displaying significant inhibition (IC<sub>50</sub> < 10  $\mu$ M) have this substitution. The replacement of chloro by other functional groups such as H, F, Br, CH<sub>3</sub>, isopropyl, and *t*-butyl leads to a decrease in binding affinity in a majority of the compounds (Table 1). Furthermore, the substitution of chloro was favorable only at the 4 position as chloro substitutions at 2 and 3 positions led to a decrease in the activity of compounds **53**, **70**, **75**, **93**, and **99** (Table 1). The results of biological activity suggest that along with R2, substitutions at R1 also modulate SENP2 inhibitory activity. The long chain O-alkyl substituents such as O-propyl, O-isopropyl, O-butyl, and O-isobutyl were preferred over short chain O-alkyl substituents such as O-methyl and O-ethyl. In fact, more than 50% of the active compounds (IC<sub>50</sub> < 30  $\mu$ M) have O-propyl, O-isopropyl, O-butyl, or O-isobutyl at the 4 position of R1 (compound **78**, **98**, **101**, **102**, and **106–112**).

The shape and electrostatic similarity to compound **38** followed by docking based prioritization resulted in 15 compounds that share the 2-phenoxy-N-[4-(2-phenoxyacetyl amino) (1,2,5-oxadiazol-3-yl)]acetamide scaffold. These compounds possess a symmetric architecture with functional groups at different positions of the phenyl ring on either side of the scaffold (R in Table 2). The biological assay results of these 15 compounds further confirmed the SENP2 inhibitory activity of the 1,2,5-oxadiazole core (Table 2). Out of the 15 compounds tested for SENP2 inhibitory activity, nine compounds (**115** and



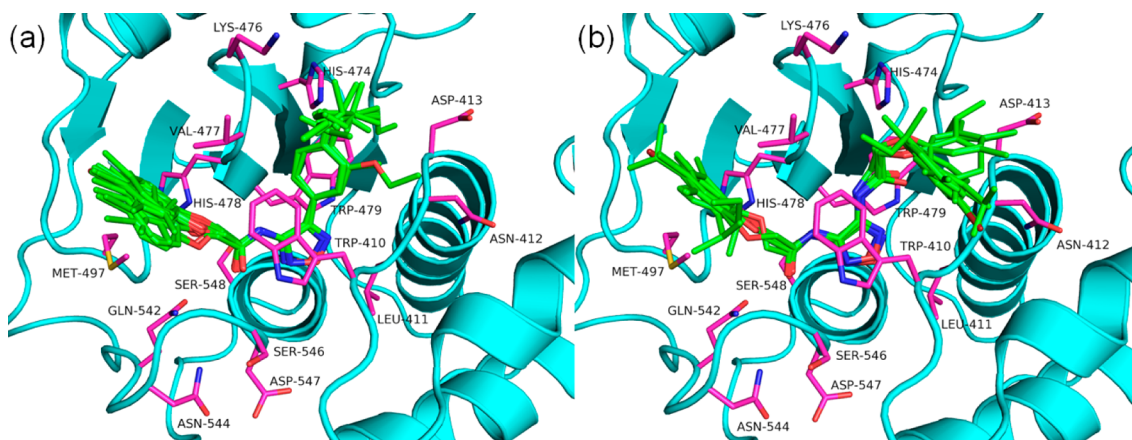


**Figure 5.** Docked binding poses of active (a) 2-phenoxy-N-(4-phenyl-1,2,5-oxadiazol-3-yl)acetamides and (b) 2-phenoxy-N-[4-(2-phenoxyacetyl-amino)(1,2,5-oxadiazol-3-yl)]acetamides.

117–124) showed an  $IC_{50}$  of  $<10 \mu M$ . Compound 117 was found to be the most active compound of the 2-phenoxy-N-[4-(2-phenoxyacetyl-amino)(1,2,5-oxadiazol-3-yl)]acetamide scaffold with an  $IC_{50}$  of  $3.7 \mu M$ . In fact, compound 117 was the most active compound among the reported 1,2,5-oxadiazoles. A similar SAR was also observed for the 2-phenoxy-N-[4-(2-phenoxyacetyl-amino)(1,2,5-oxadiazol-3-yl)]acetamide scaffold, and the presence of chloro at position 4 led to higher activity (compound 117, 120, and 121).

The active compounds from both 1,2,5-oxadiazoles scaffolds (compound 52, 54, 59, 68, 69, 78, 82–85, 91, 98, 101, 102, 106–112, 115–124, 128, and 129) were also tested against the closely related isoform SENP1. These compounds were expected to display some affinity for SENP1 also as the catalytic site of these two proteins is quite conserved (Figure S3). As shown in Tables 1 and 2, most of the compounds inhibited SENP1 with matching potency as for SENP2, which further confirms the utility of 1,2,5-oxadiazoles as general SENP inhibitors.

We next evaluated the specificity of 1,2,5-oxadiazoles for SENP by investigating their ability to inhibit the peptidase activity of a cysteine protease papain and a serine protease trypsin. The peptidase activity of papain and trypsin in the presence of  $100 \mu M$  compounds 52, 54, 59, 68, 69, 78, 82–85, 91, 98, 101, 102, 106–112, 115–124, 128, and 129 was measured using a FRET based assay for papain and trypsin. The results revealed that the majority of compounds except compounds 120 and 121 exhibit selectivity for SENP over papain and trypsin (Tables 1 and 2). Although compounds 120 and 121 did not inhibit trypsin, they did inhibit around 40% of the activity of another cysteine protease papain at a concentration of  $100 \mu M$ .

The FRET based biological assay revealed a few 1,2,5-oxadiazoles with 2-phenoxy-N-(4-phenyl-1,2,5-oxadiazol-3-yl)acetamides and 2-phenoxy-N-[4-(2-phenoxyacetyl-amino)(1,2,5-oxadiazol-3-yl)]acetamides as potent inhibitors of SENP2. To gain insight into the structural basis of SENP2 inhibition by these chemical classes, the docking predicted binding mode of potent compounds ( $IC_{50} < 10 \mu M$ ) of both scaffolds in the catalytic site of SENP2 was investigated. Figure 5 presents the Glide-XP predicted binding modes of 2-phenoxy-N-(4-phenyl-1,2,5-oxadiazol-3-yl)acetamides (compounds 52, 59, 68, 69, 78, 91, 98, 101, 102, 106–109, and 111) and 2-phenoxy-N-[4-(2-phenoxyacetyl-amino)(1,2,5-oxa-

diazol-3-yl)]acetamides (compounds 115 and 117–124). As can be seen in Figure 5, both scaffolds are predicted to bind to SENP2 in a very similar manner, sharing all critical interactions. The 1,2,5-oxadiazole ring in all the compounds was found to be stacked between Trp410 and Trp479 amino acid residues. The stacking between two tryptophans help positioning compounds to facilitate hydrogen bonding with the backbone carbonyl of Val477 (Figure 5). The binding was also stabilized by hydrophobic contacts between side chains of Trp410 and Val477 with the phenyl ring in 2-phenoxy-N-(4-phenyl-1,2,5-oxadiazol-3-yl)acetamides and the phenoxy acetamide group in phenoxy acetamides. Additionally, the hydrocarbon chain of Met497 makes good contacts with the phenoxy acetamide moiety in both scaffolds.

Finally, to access the suitability of 1,2,5-oxadiazoles for therapeutic purposes, their physicochemical and ADME properties were predicted using QikProp<sup>58</sup> and are reported in Supporting Information Table 1. The results show that almost all active compounds of two 1,2,5-oxadiazole scaffolds displayed predicted properties in the range for 95% of known oral drugs. Both 2-phenoxy-N-(4-phenyl-1,2,5-oxadiazol-3-yl)acetamide and 2-phenoxy-N-[4-(2-phenoxyacetyl-amino)(1,2,5-oxadiazol-3-yl)]acetamide scaffolds were predicted to have good solubility, metabolism, cell permeation, and bioavailability. None of the compounds was predicted to bind human serum albumin and block HERG  $K^+$  channels. Although the predicted Caco2 cell permeability (QPPCaco2) values for both 1,2,5-oxadiazole scaffolds are within range for 95% of known oral drugs, 2-phenoxy-N-(4-phenyl-1,2,5-oxadiazol-3-yl)acetamides (compounds 43, 50–114) were predicted to have better absorption than 2-phenoxy-N-[4-(2-phenoxyacetyl-amino)(1,2,5-oxadiazol-3-yl)]acetamides (compounds 38, 115–129). Further, both 1,2,5-oxadiazole scaffolds were predicted to have good blood–brain penetration and skin permeability. As far as physicochemical properties are concerned, no Lipinski's "rule of five"<sup>59</sup> violations were observed for both 2-phenoxy-N-(4-phenyl-1,2,5-oxadiazol-3-yl)acetamide and 2-phenoxy-N-[4-(2-phenoxyacetyl-amino)(1,2,5-oxadiazol-3-yl)]acetamide scaffolds, indicating the drug-likeness of these 1,2,5-oxadiazoles.

## CONCLUSION

Our hierarchical virtual screening approach including shape similarity, electrostatic potential similarity, and molecular

docking steered the identification of two scaffolds containing the 1,2,5-oxadiazole core as a novel class of SENP2 inhibitors. The reported chemical class displayed moderate inhibition of SENP2 and SENP1 endopeptidase activity without affecting activities of other cysteine and serine proteases, papain and trypsin. The structure activity relationship around 2-phenoxy-N-(4-phenyl-1,2,5-oxadiazol-3-yl)acetamide and 2-phenoxy-N-[4-(2-phenoxyacetyl amino)(1,2,5-oxadiazol-3-yl)]acetamides scaffolds reveals the crucial role of electron withdrawing groups at the 4 position for significant SENP2 inhibitory activities. Furthermore, computational analysis has provided some insights into the binding mode of this class of inhibitors. Although the reported molecules showed only moderate potencies, the novel and selective nature of this chemical class makes them good candidates for future development into highly potent SENP inhibitors through medicinal chemistry optimization.

## ■ ASSOCIATED CONTENT

### ■ Supporting Information

Three additional figures: (1) Correlation between Glide-XP score and molecular weight. (2) Docking predicted binding mode of virtual screening hits belonging to 1,2,5-oxadiazoles. (3) Sequence alignment between catalytic domain of SENP1 and SENP2. One additional table: (1) The physicochemical and predicted ADME properties of active 1,2,5-oxadiazoles. This material is available free of charge via the Internet at <http://pubs.acs.org>.

## ■ AUTHOR INFORMATION

### Corresponding Author

\*Phone: +81-48-467-8792. Fax: +81-48-467-8790. E-mail: [kamzhang@riken.jp](mailto:kamzhang@riken.jp).

### Author Contributions

<sup>†</sup>These authors contributed equally.

### Notes

The authors declare no competing financial interest.

## ■ ACKNOWLEDGMENTS

We thank RIKEN Integrated Cluster of Clusters (RICC) for the supercomputing resources provided for this study. We thank members of Zhang Initiative Research Unit for help and discussions. This work was supported in part by the Initiative Research Unit program and the Chemical Genomics Research Project, RIKEN ASI, the CREST Research Project, the Japan Science and Technology Corporation, and a Grant-in-Aid for Scientific Research (C) and on Priority Area "Cancer" from the Ministry of Education, Culture, Sports, Science and Technology of Japan.

## ■ REFERENCES

- (1) Zhao, J. Sumoylation regulates diverse biological processes. *Cell Mol. Life Sci.* **2007**, *64*, 3017–3033.
- (2) Tang, Z.; Hecker, C. M.; Scheschonka, A.; Betz, H. Protein interactions in the sumoylation cascade: lessons from X-ray structures. *FEBS J.* **2008**, *275*, 3003–3015.
- (3) Sarge, K. D.; Park-Sarge, O. K. Sumoylation and human disease pathogenesis. *Trends Biochem. Sci.* **2009**, *34*, 200–205.
- (4) Yeh, E. T. SUMOylation and De-SUMOylation: wrestling with life's processes. *J. Biol. Chem.* **2009**, *284*, 8223–8227.
- (5) Gareau, J. R.; Lima, C. D. The SUMO pathway: emerging mechanisms that shape specificity, conjugation and recognition. *Nat. Rev. Mol. Cell Biol.* **2010**, *11*, 861–871.
- (6) Lois, L. M.; Lima, C. D. Structures of the SUMO E1 provide mechanistic insights into SUMO activation and E2 recruitment to E1. *EMBO J.* **2005**, *24*, 439–451.
- (7) Olsen, S. K.; Capili, A. D.; Lu, X.; Tan, D. S.; Lima, C. D. Active site remodelling accompanies thioester bond formation in the SUMO E1. *Nature* **2010**, *463*, 906–912.
- (8) Lu, X.; Olsen, S. K.; Capili, A. D.; Cisar, J. S.; Lima, C. D.; Tan, D. S. Designed semisynthetic protein inhibitors of Ub/Ubl E1 activating enzymes. *J. Am. Chem. Soc.* **2010**, *132*, 1748–1749.
- (9) Mukhopadhyay, D.; Dasso, M. Modification in reverse: the SUMO proteases. *Trends Biochem. Sci.* **2007**, *32*, 286–295.
- (10) Hay, R. T. SUMO-specific proteases: a twist in the tail. *Trends Cell Biol.* **2007**, *17*, 370–376.
- (11) Drag, M.; Salvesen, G. S. DeSUMOylating enzymes–SENPs. *IUBMB Life* **2008**, *60*, 734–742.
- (12) Zuo, Y.; Cheng, J.-K. Small ubiquitin-like modifier protein-specific protease 1 and prostate cancer. *Asian J. Androl.* **2009**, *11*, 36–38.
- (13) Bawa-Khalife, T.; Cheng, J.; Lin, S. H.; Ittmann, M. M.; Yeh, E. T. SENP1 induces prostatic intraepithelial neoplasia through multiple mechanisms. *J. Biol. Chem.* **2010**, *285*, 25859–25866.
- (14) Cheng, J.; Kang, X.; Zhang, S.; Yeh, E. T. SUMO-specific protease 1 is essential for stabilization of HIF1α during hypoxia. *Cell* **2007**, *131*, 584–595.
- (15) Yamaguchi, T.; Sharma, P.; Athanasiou, M.; Kumar, A.; Yamada, S.; Kuehn, M. R. Mutation of SENP1/SuPr-2 reveals an essential role for desumoylation in mouse development. *Mol. Cell. Biol.* **2005**, *25*, 5171–5182.
- (16) Cheng, J.; Bawa, T.; Lee, P.; Gong, L.; Yeh, E. T. Role of desumoylation in the development of prostate cancer. *Neoplasia* **2006**, *8*, 667–676.
- (17) Jacques, C.; Baris, O.; Prunier-Mirebeau, D.; Savagner, F.; Rodien, P.; Rohmer, V.; Franc, B.; Guyetant, S.; Malthiery, Y.; Reynier, P. Two-step differential expression analysis reveals a new set of genes involved in thyroid oncogenic tumors. *J. Clin. Endocrinol. Metab.* **2005**, *90*, 2314–2320.
- (18) Xu, Y.; Li, J.; Zuo, Y.; Deng, J.; Wang, L. S.; Chen, G. Q. SUMO-specific protease 1 regulates the in vitro and in vivo growth of colon cancer cells with the upregulated expression of CDK inhibitors. *Cancer Lett.* **2011**, *309*, 78–84.
- (19) Heo, K. S.; Chang, E.; Le, N. T.; Cushman, H.; Yeh, E. T.; Fujiwara, K.; Abe, J. De-SUMOylation Enzyme of Sentrin/SUMO-Specific Protease 2 Regulates Disturbed Flow-Induced SUMOylation of ERK5 and p53 that Leads to Endothelial Dysfunction and Atherosclerosis. *Circ. Res.* **2013**, *112*, 911–923.
- (20) Kim, E. Y.; Chen, L.; Ma, Y.; Yu, W.; Chang, J.; Moskowitz, I. P.; Wang, J. Enhanced desumoylation in murine hearts by overexpressed SENP2 leads to congenital heart defects and cardiac dysfunction. *J. Mol. Cell. Cardiol.* **2012**, *52*, 638–649.
- (21) Chiu, S. Y.; Asai, N.; Costantini, F.; Hsu, W. SUMO-specific protease 2 is essential for modulating p53-Mdm2 in development of trophoblast stem cell niches and lineages. *PLoS Biol.* **2008**, *6*, e310.
- (22) Jiang, M.; Chiu, S. Y.; Hsu, W. SUMO-specific protease 2 in Mdm2-mediated regulation of p53. *Cell Death Differ.* **2011**, *18*, 1005–1015.
- (23) Shen, H. J.; Zhu, H. Y.; Yang, C.; Ji, F. SENP2 regulates hepatocellular carcinoma cell growth by modulating the stability of beta-catenin. *Asian Pac. J. Cancer Prev.* **2012**, *13*, 3583–3587.
- (24) Hemelaar, J.; Borodovsky, A.; Kessler, B. M.; Reverter, D.; Cook, J.; Kolli, N.; Gan-Erdene, T.; Wilkinson, K. D.; Gill, G.; Lima, C. D.; Ploegh, H. L.; Ova, H. Specific and covalent targeting of conjugating and deconjugating enzymes of ubiquitin-like proteins. *Mol. Cell. Biol.* **2004**, *24*, 84–95.
- (25) Borodovsky, A.; Ova, H.; Meester, W. J.; Venanzi, E. S.; Bogoy, M. S.; Hekking, B. G.; Ploegh, H. L.; Kessler, B. M.; Overkleeft, H. S. Small-molecule inhibitors and probes for ubiquitin- and ubiquitin-like-specific proteases. *ChemBioChem.* **2005**, *6*, 287–291.
- (26) Albrow, V. E.; Ponder, E. L.; Fasci, D.; Bekes, M.; Deu, E.; Salvesen, G. S.; Bogoy, M. Development of small molecule inhibitors

and probes of human SUMO deconjugating proteases. *Chem. Biol.* **2011**, *18*, 722–732.

(27) Qiao, Z.; Wang, W.; Wang, L.; Wen, D.; Zhao, Y.; Wang, Q.; Meng, Q.; Chen, G.; Wu, Y.; Zhou, H. Design, synthesis, and biological evaluation of benzodiazepine-based SUMO-specific protease 1 inhibitors. *Bioorg. Med. Chem. Lett.* **2011**, *21*, 6389–6392.

(28) Dobrota, C.; Fasci, D.; Hadade, N. D.; Roiban, G. D.; Pop, C.; Meier, V. M.; Dumitru, I.; Matache, M.; Salvesen, G. S.; Funeriu, D. P. Glycine fluoromethylketones as SENP-specific activity based probes. *ChemBioChem.* **2012**, *13*, 80–84.

(29) Uno, M.; Koma, Y.; Ban, H. S.; Nakamura, H. Discovery of 1-[4-(N-benzylamino)phenyl]-3-phenylurea derivatives as non-peptidic selective SUMO-sentrin specific protease (SENP)1 inhibitors. *Bioorg. Med. Chem. Lett.* **2012**, *22*, 5169–5173.

(30) Chen, Y.; Wen, D.; Huang, Z.; Huang, M.; Luo, Y.; Liu, B.; Lu, H.; Wu, Y.; Peng, Y.; Zhang, J. 2-(4-Chlorophenyl)-2-oxoethyl 4-benzamidobenzoate derivatives, a novel class of SENP1 inhibitors: Virtual screening, synthesis and biological evaluation. *Bioorg. Med. Chem. Lett.* **2012**, *22*, 6867–6870.

(31) Madu, I. G.; Namanja, A. T.; Su, Y.; Wong, S.; Li, Y. J.; Chen, Y. Identification and Characterization of a New Chemotype of Noncovalent SENP Inhibitors. *ACS Chem. Biol.* **2013**, *8* (7), 1435–1441.

(32) Reverter, D.; Lima, C. D. Structural basis for SENP2 protease interactions with SUMO precursors and conjugated substrates. *Nat. Struct. Mol. Biol.* **2006**, *13*, 1060–1068.

(33) ROCS, version 3.1.2; OpenEye Scientific Software, Inc.: Santa Fe, NM, 2011; [www.eyesopen.com](http://www.eyesopen.com).

(34) EON, version 2.1.0; OpenEye Scientific Software, Inc.: Santa Fe, NM, 2011; [www.eyesopen.com](http://www.eyesopen.com).

(35) Halgren, T. A. Merck molecular force field. I. Basis, form, scope, parameterization, and performance of MMFF94. *J. Comput. Chem.* **1996**, *17*, 490–519.

(36) Halgren, T. A. Merck molecular force field. II. MMFF94 van der Waals and electrostatic parameters for intermolecular interactions. *J. Comput. Chem.* **1996**, *17*, 520–552.

(37) Maestro, version 9.2; Schrödinger, LLC: New York, 2011.

(38) LigPrep, version 2.5; Schrödinger, LLC: New York, 2011.

(39) Jorgensen, W. L.; Tirado-Rives, J. The OPLS [optimized potentials for liquid simulations] potential functions for proteins, energy minimizations for crystals of cyclic peptides and crambin. *J. Am. Chem. Soc.* **1988**, *110*, 1657–1666.

(40) Jorgensen, W. L.; Maxwell, D. S.; Tirado-Rives, J. Development and Testing of the OPLS All-Atom Force Field on Conformational Energetics and Properties of Organic Liquids. *J. Am. Chem. Soc.* **1996**, *118*, 11225–11236.

(41) Glide, version 5.7; Schrödinger, LLC: New York, 2011.

(42) Friesner, R. A.; Banks, J. L.; Murphy, R. B.; Halgren, T. A.; Klicic, J. J.; Mainz, D. T.; Repasky, M. P.; Knoll, E. H.; Shelley, M.; Perry, J. K.; Shaw, D. E.; Francis, P.; Shenkin, P. S. Glide: a new approach for rapid, accurate docking and scoring. 1. Method and assessment of docking accuracy. *J. Med. Chem.* **2004**, *47*, 1739–1749.

(43) Friesner, R. A.; Murphy, R. B.; Repasky, M. P.; Frye, L. L.; Greenwood, J. R.; Halgren, T. A.; Sanschagrin, P. C.; Mainz, D. T. Extra precision glide: docking and scoring incorporating a model of hydrophobic enclosure for protein-ligand complexes. *J. Med. Chem.* **2006**, *49*, 6177–6196.

(44) Halgren, T. A.; Murphy, R. B.; Friesner, R. A.; Beard, H. S.; Frye, L. L.; Pollard, W. T.; Banks, J. L. Glide: a new approach for rapid, accurate docking and scoring. 2. Enrichment factors in database screening. *J. Med. Chem.* **2004**, *47*, 1750–1759.

(45) The PyMOL Molecular Graphics System, version 1.5.0.4; Schrödinger, LLC: New York.

(46) Liu, Y.; Song, Y.; Madahar, V.; Liao, J. Quantitative Forster resonance energy transfer analysis for kinetic determinations of SUMO-specific protease. *Anal. Biochem.* **2012**, *422*, 14–21.

(47) Naylor, E.; Arredouani, A.; Vasudevan, S. R.; Lewis, A. M.; Parkesh, R.; Mizote, A.; Rosen, D.; Thomas, J. M.; Izumi, M.; Ganesan,

A.; Galione, A.; Churchill, G. C. Identification of a chemical probe for NAADP by virtual screening. *Nat. Chem. Biol.* **2009**, *5*, 220–226.

(48) Hevener, K. E.; Mehboob, S.; Su, P. C.; Truong, K.; Boci, T.; Deng, J.; Ghassemi, M.; Cook, J. L.; Johnson, M. E. Discovery of a novel and potent class of *F. tularensis* enoyl-reductase (FabI) inhibitors by molecular shape and electrostatic matching. *J. Med. Chem.* **2012**, *55*, 268–279.

(49) Kaoud, T. S.; Yan, C.; Mitra, S.; Tseng, C. C.; Jose, J.; Taliaferro, J. M.; Tuohetahuntala, M.; Devkota, A.; Sammons, R.; Park, J.; Park, H.; Shi, Y.; Hong, J.; Ren, P.; Dalby, K. N. From in Silico Discovery to intra-Cellular Activity: Targeting JNK-Protein Interactions with Small Molecules. *ACS Med. Chem. Lett.* **2012**, *3*, 721–725.

(50) Kirchmair, J.; Distinto, S.; Markt, P.; Schuster, D.; Spitzer, G. M.; Liedl, K. R.; Wolber, G. How To Optimize Shape-Based Virtual Screening: Choosing the Right Query and Including Chemical Information. *J. Chem. Inf. Model.* **2009**, *49*, 678–692.

(51) Tawa, G.; Baber, J. C.; Humblet, C. Computation of 3D queries for ROCS based virtual screens. *J. Comput.-Aided Mol. Des.* **2009**, *23*, 853–868.

(52) Sato, T.; Yuki, H.; Takaya, D.; Sasaki, S.; Tanaka, A.; Honma, T. Application of Support Vector Machine to Three-Dimensional Shape-Based Virtual Screening Using Comprehensive Three-Dimensional Molecular Shape Overlay with Known Inhibitors. *J. Chem. Inf. Model.* **2012**, *52*, 1015–1026.

(53) Brenke, R.; Kozakov, D.; Chuang, G. Y.; Beglov, D.; Hall, D.; Landon, M. R.; Mattos, C.; Vajda, S. Fragment-based identification of druggable 'hot spots' of proteins using Fourier domain correlation techniques. *Bioinformatics* **2009**, *25*, 621–627.

(54) OMEGA, version 2.4.6; OpenEye Scientific Software, Inc.: Santa Fe, NM, 2012; [www.eyesopen.com](http://www.eyesopen.com).

(55) Hawkins, P. C.; Skillman, A. G.; Warren, G. L.; Ellingson, B. A.; Stahl, M. T. Conformer generation with OMEGA: algorithm and validation using high quality structures from the Protein Databank and Cambridge Structural Database. *J. Chem. Inf. Model.* **2010**, *50*, 572–584.

(56) Hawkins, P. C.; Nicholls, A. Conformer generation with OMEGA: learning from the data set and the analysis of failures. *J. Chem. Inf. Model.* **2012**, *52*, 2919–2936.

(57) Rogers, D. J.; Tanimoto, T. T. A Computer Program for Classifying Plants. *Science* **1960**, *132*, 1115–1118.

(58) QikProp, version 3.4; Schrödinger, LLC: New York, 2011.

(59) Lipinski, C. A.; Lombardo, F.; Dominy, B. W.; Feeney, P. J. Experimental and computational approaches to estimate solubility and permeability in drug discovery and development settings. *Adv. Drug Delivery. Rev.* **2001**, *46*, 3–26.